Available online at www.sciencedirect.com
SCIENCE DIRECT®
Journal of Catalysis 218 (2003) 67–77
JOURNAL OF CATALYSIS
www.elsevier.com/locate/jcat

A study of $Cu/ZnO/Al_2O_3$ methanol catalysts prepared by flame combustion synthesis

J.R. Jensen,[1] T. Johannessen, S. Wedel, and H. Livbjerg *

Interdisciplinary Research Centre for Catalysis (ICAT), Department of Chemical Engineering, Technical University of Denmark, DK-2800 Lyngby, Denmark

Received 25 September 2002; revised 17 January 2003; accepted 20 January 2003

Abstract

The flame combustion synthesis of $Cu/ZnO/Al_2O_3$ catalysts for the synthesis of methanol from CO, CO_2, and H_2 is investigated. The oxides are generated in a premixed flame from the acetylacetonate vapours of Cu, Zn, and Al mixed with the fuel and air prior to combustion. The flame-generated powder is examined by X-ray powder diffraction, determination of the specific surface area by the BET method, determination of the copper dispersion in the reduced catalyst by a novel N_2O method, transmission electron microscopy, and testing of the catalytic properties in a catalytic microreactor. A low peak temperature and quench cooling of the flame tend to increase the dispersion of the phases and the specific surface area of the particles. Properties of both the ternary composition, the three binary compositions, and the pure oxides are discussed. The calculation of simultaneous phase and chemical equilibrium is used in the assessment of the phase composition of the particles. The specific surface area varies from 100 m^2/g or a little below for samples without Al to several hundred m^2/g for the respective compositions of pure Al_2O_3 and $ZnAl_2O_4$. Copper dispersion after reduction varies from 1.8 to 14.1%. A ternary catalyst with the composition of Cu:Zn:Al = 45:45:10 has the highest catalytic activity of all samples tested. This catalyst is also very selective and stable toward thermal deactivation. The role of the individual catalyst components in the optimal catalyst is discussed.

Keywords: Aerosols; Nanoparticles; Flame synthesis; CuO; ZnO; Al_2O_3; Methanol; Catalyst

1. Introduction

Small nanoparticles of metal oxides can be generated by flame combustion of volatile precursors. The so-called flame combustion synthesis, already widely used for materials like carbon black, fumed silica, and titania [1,2], provides an alternative route to catalyst manufacture as recently demonstrated by Stark et al. [3] for V_2O_5/TiO_2 composite particles with excellent catalytic properties in the SCR process and by Johannessen and Koutsopoulos [4] for a Pt/TiO_2 catalyst for SO_2 oxidation.

Flame synthesis is particularly effective for the generation of those material structures, which are inherently important in heterogeneous catalysis, i.e., high specific surface areas for composite materials and nanostructured phase distribution. Jensen et al. [5] showed how to produce $ZnAl_2O_4$ spinel with a high surface area by co-combustion of volatile Zn- and Al-acetylacetonates. The combination of mixing at the molecular level and an extreme supersaturation for the metal-oxide molecules formed by combustion ensures the formation of a spinel phase with a high surface area during the few milliseconds of residence time in the high-temperature zone. The traditional wet methods which apply (co-)precipitation are far more difficult to control and require subsequent calcination, which is accompanied by an unavoidable loss of surface area.

This investigation expands the zinc-aluminate synthesis by the methods of [5] to the flame synthesis of the ternary $CuO/ZnO/Al_2O_3$ samples for the synthesis of methanol. The $Cu/ZnO/Al_2O_3$ catalyst system was chosen since it is known to be structure sensitive [6]. A novel synthesis route may lead to unexpected and unique catalyst properties. Furthermore, the system is rather well investigated, which is advantageous for the characterisation of a new route of synthesis.

* Corresponding author.
E-mail address: hl@olivia.kt.dtu.dk (H. Livbjerg).
[1] Present address: Haldor Topsøe A/S, DK-2800 Lyngby, Denmark.

0021-9517/03/$ – see front matter
doi:10.1016/S0021-9517(03)00047-2

The mechanisms of flame aerosol synthesis

During combustion in the flame zone the precursor species are decomposed at high temperatures. The products are released as vapour molecules, which form particle seeds by nucleation, when they become supersaturated during cooling of the flue gas. The particle seeds grow by condensation of supersaturated vapours and by coagulation following interparticle collisions. Concomitantly with particle growth, processes within the single particles alter their shape toward compact forms (sintering) and rearrange the phase composition toward stable crystalline phases by crystal nucleation and growth. A special case arises when fast combustion reactions generate molecules into a state of extreme supersaturation, which is often followed by collision-limited growth of particles, leading ultimately to very high specific surface areas. For more volatile species, condensation occurs after the temperature eventually has reached the saturation point. In multicomponent mixtures, the individual components may condense consecutively, each in its own temperature range.

The specific surface area, particle morphology, and crystalline structure of the particles can be altered by changing, e.g., the flame peak temperature, the high-temperature zone residence time, and the precursor concentration. These conditions can be varied within wide limits for a given burner and further expanded by employing different burner types and geometries. Pratsinis [1], Jensen et al. [5], and Jensen [7] provide further details about flame synthesis and references to the relevant literature.

2. Experimental

2.1. Flame reactor setup

$CuO/ZnO/Al_2O_3$ samples are prepared by combustion synthesis from the volatile precursors consisting of the acetylacetonates of copper, zinc, and aluminum. The flame reactor has been designed to obtain particles with large specific surface areas. A high surface area is favoured by a low precursor vapour pressure [5], which is obtained in this reactor by the combustion of a homogeneous gas in which N_2, O_2, and H_2 (or CH_4) are well mixed with the volatile catalyst precursors prior to ignition. The reactor is also provided with means for the optional quench cooling of the flame by the injection of jets of cold air downstream from the ignition zone. The particles therefore are exposed to the peak temperatures only as long as necessary for the generation of the desired molecular structures, which reduces the effect of sintering of the coagulated particles [8]. Details of the reactor setup are shown in Fig. 1.

The reactor feed is mixed from separately controlled flows of fuel (H_2 or CH_4), air, and three separate lines with nitrogen carrier gas containing the precursor vapours. Each precursor line passes a sublimation unit for the controlled

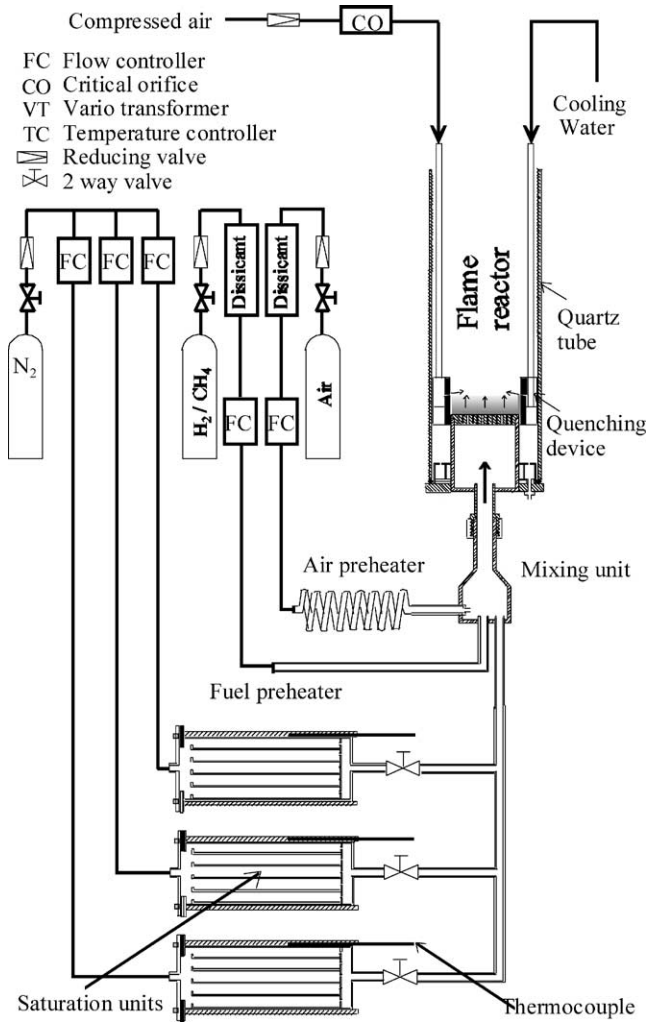

Fig. 1. Flame reactor system with fuel, air, and precursor feed lines.

addition of the vapours of the acetylacetonate of copper, zinc, and aluminum, respectively. The precursor powders are distributed on horizontal trays encased in thermostated aluminum boxes with sufficient gas contact to ensure saturation of the effluent gas with precursor vapours. The vapour content in the precursor lines is thus independent of the flow rate of carrier gas and can be controlled by the temperature of the sublimation unit. The vapour pressures of the precursors are determined from the precursor weight loss for a given volume of carrier gas and are shown in Fig. 2 as a function of temperature. Any desired ternary particle composition is obtainable by the proper combination of saturator temperatures and carrier gas flow rates. Temperatures in the range of 90–180 °C have been adequate for the present experiments. The copper precursor has the lowest vapour pressure and its saturation unit was operated solely at its maximum temperature of 180 °C. Above 200 °C the precursor starts to decompose. All gas lines containing precursor vapours are heated to 200 °C to prevent condensation.

Prior to combustion all feed lines are intimately mixed in a swirl mixer. Combustion occurs in a flat flame stabi-

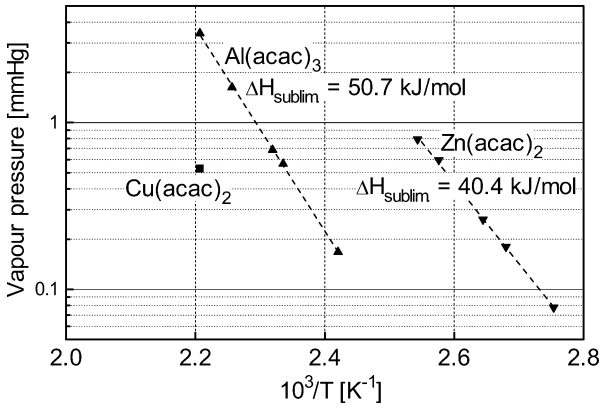

Fig. 2. The vapour pressures of Cu, Al, and Zn acetylacetonate as a function of temperature. The vapour pressures are determined from the weight loss of the saturator units due to sublimation of the precursors. The sublimation enthalpies for Al- and Zn-acetylacetonate are estimated based on the linear correlation between $1/T$ and the vapour pressure.

lized by a flame arrestor—a stainless-steel plate of diameter 36 mm perforated by numerous small holes. A cylindrical quartz tube of length 200 mm and inner diameter of 67 mm surrounds the flame and shields it from intrusion of the ambient air.

A ring, which can be positioned at any given height above the flame, is placed inside the quartz shield and holds the nozzles for quench cooling of the flame by cold air. The design of the quench-cooling device is very critical since the nozzles must give the jets of cold air a slightly upward and off-axis direction to create a stabilizing swirl that prevents the complete distortion of the flame, which would otherwise occur [8]. This special configuration enables us to quench cool directly above the flame front without disturbing the flame below the quenching level.

Inhalation of small particles is potentially health hazardous, so for safety reasons the entire setup is placed in a fume hood.

It is principally the temperature–time history and the concentration of precursor vapours of the reacting flow in the flame which determine the properties of the effluent aerosol particles. Both sets of flame conditions can be altered within wide limits to achieve advantageous particle properties. Table 1 summarizes the experimental design for the thermal flame conditions, which are altered systematically by switching on or off the quench cooling and by a change from a lean hydrogen mixture to a rich methane fuel mixture. The corresponding axial temperature profiles for the four selected conditions are shown in Fig. 3. They are measured with a platinum–platinum/10% rhodium thermocouple with 0.3-mm free wires and a welding bead with diameter 1.3 mm and corrected for radiation influence [7]. The four different conditions in Table 1 and Fig. 3 combine a significant variation of the peak temperature—high for methane and low for hydrogen—with a similarly significant variation in the flame-cooling rate—a high rate with quench cooling and low rate without. The methane flame with and without quench

Table 1
Flame operating conditions

	Flame			
	1 (CH_4)	2 (CH_4, quench)	3 (H_2)	4 (H_2, quench)
Air (dm^3/min)[c]	10.1	10.1	10.1	10.1
Methane (dm^3/min)[c]	0.986	0.986	0	0
Hydrogen (dm^3/min)[c]	0	0	1.71	1.71
Quenched air[a] (dm^3/min)[c]	0	5.2	0	5.2
Oxygen/methane ratio	2.15	2.15	–	–
Oxygen/hydrogen ratio	–	–	1.24	1.24
Peak temperature (°C)[b]	1464	1398	995	954

[a] The quench jets are positioned 12.5 mm above the flame arrestor.
[b] Measured peak temperature corrected for radiation loss.
[c] All flows are given at 20 °C, 1 atm. The carrier gas through the Al-, Cu-, and Zn-(acac) saturators varies between 0 and 1 dm^3/min, depending on the desired composition.

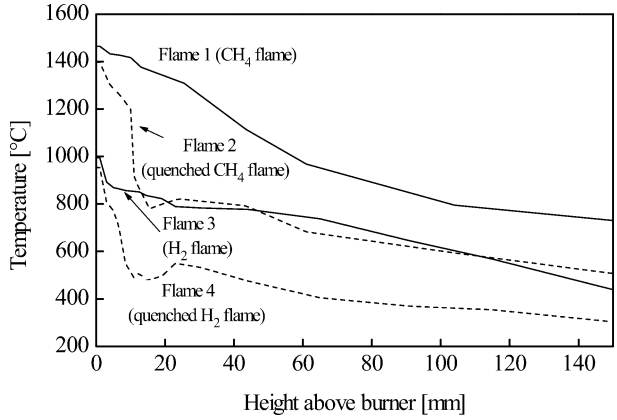

Fig. 3. Flame temperature profiles measured along the center line of the burner for the selected standard test conditions (cf. Table 1), which are designed to vary systematically with respect to peak temperature and cooling rate.

cooling are compared in the photos of Fig. 4. The green light emitted by Cu above approximately 1000 °C illustrates the changes in the high-temperature zone, which extends high above the flame front without quench cooling (a) but is confined to the region below the ring during quench cooling (b).

The powder produced in the flame is collected on a 47-mm polycarbonate filter with 1-μm pores through which the effluent gas is withdrawn by a vacuum pump after being cooled to 70 °C. The particles are subjected to the following examinations:

The BET surface area is measured by multipoint nitrogen adsorption (Gemini 2630, Micromeritics) at 77 K. An equivalent primary particle diameter can be estimated from the BET surface S_A by

$$d_{BET} = \frac{6}{\rho_p S_A},$$

where ρ_p is the solid phase density.

X-ray diffraction (XRD) is obtained with a Cu-K_α radiation diffractometer (Philips PW1820/3711). The diffrac-

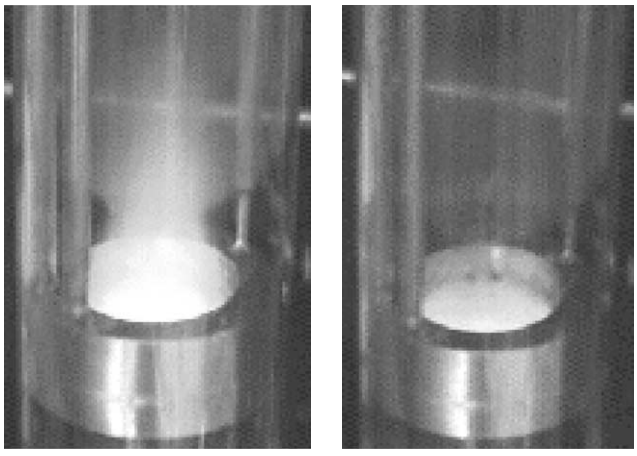

(a) (b)

Fig. 4. Photograph of the flame reactor which illustrates the changes in the high-temperature zone during quench cooling. The flame contains Cu, which emits green light above approximately 1000 °C. (a) Methane–air flame and (b) quenched methane–air flame.

tograms can be measured expediently directly on the particle filter cake subject to a correction for a weak background signal from the filter material. Crystallite dimensions in different crystal directions were estimated from line broadening using the Scherrer equation [9]. The peak widths at half height were estimated by fitting the peaks to a multiple Gaussian distribution using a least-squares method. When the crystallite size gradually becomes smaller, line broadening eventually dominates the diffractogram, which hence cannot be resolved reasonably. In this case the material appears X-ray amorphous, although in many cases more or less perfect nanocrystalline particles and phases may presumably be present. Further details of the XRD analysis are shown in [7].

Transmission electron microscopy (TEM) is used for particles sampled directly from the hot gas by diffusional and thermophoretic[2] deposition on 300-μm mesh Ni TEM grids with carbon film. The grid is inserted manually by means of pincers for 5–10 s at the center line of the flame approximately 100 mm above the diffuser. A Philips 300-kV TEM was used to image the particles and to measure the overall chemical composition by EDAX (energy-dispersive X-ray analysis).

Copper dispersion[3] is measured with the N_2O method in which N_2O is assumed to react with the surface copper atoms selectively by the reaction $2Cu + N_2O \rightarrow Cu_2O + N_2$ [10–12]. We have developed a novel adaption of the N_2O method by which the transient evolvement of N_2 in a microreactor is used to compute the concentration of surface Cu after a correction for a slow diffusion of O into the bulk material. The measurements are made at ambient pressure with a constant flow of gas through a fixed bed of catalyst particles by switching the feed gas composition from pure helium to 2% N_2O in helium. The effluent gas passes through a freeze trap with liquid nitrogen, which selectively removes unreacted N_2O from the gas. Nitrogen evolved by the oxidation reaction can then be determined accurately by a calibrated thermal conductivity detector. Prior to the measurements the samples are reduced in pure hydrogen for 1 h at 220 °C. The method is suitable for the small amounts of catalyst of the present investigation and is applied to the particles in situ in the catalytic test reactor described below. It was proved that the N_2O treatment does not change the catalytic activity or the Cu dispersion. The N_2O treatment is made at 90 °C with 2% (mol/mol) N_2O in He. Pretreatment of the sample, reduction, etc., is made according to the procedures described in [7].

2.2. Catalyst tests

Measurements of the catalytic properties are made with the catalytic microreactor shown in Fig. 5. A small amount of powder sample ($\sim$ 20 mg) collected from the flame generator is transferred to a Pyrex glass capillary tube with an internal diameter of 2 mm so that it forms a small bed held in place by quartz wool plugs at one end of the tube. A constriction made in the wall of the capillary tube stabilizes the innermost wool plug, positioned at the gas outlet from the bed (cf. Fig. 5)

When a catalyst is tested, its capillary tube is mounted in a cylindrical recess sealed by Viton o-rings at the upper part of the reactor assembly. When the reactor is reassembled, the capillary tube is encased in a cylindrical steel jacket. The feed gas mixture enters through the cylindrical annulus between the capillary tube and the surrounding steel jacket in downward flow and passes the catalyst bed, leaving the reactor in upward flow internally in the capillary tube. The steel jacket fits into a hole bored in a thermostated cylindrical block of aluminum–bronze so that one end, containing the catalyst, is held isothermal due to the high heat conductivity of the bronze, while the other end protrudes outside the bronze block and is kept at a lower temperature to protect the Viton o-ring seals and inlet and outlet gas tubing connections. The reactor operation is trouble-free for catalyst temperatures up to 400 °C.

Due to the miniature catalyst bed and the high heat conductivity of the bronze block, the reactor and the catalyst bed stay effectively isothermal, which has been confirmed by measurements of the gas exit temperatures with thin thermocouples inserted into the capillary tube.

The reactor material is nickel-free steel. The high-temperature zone of the steel jacket is furthermore lined internally with copper. These materials are necessary to avoid formation of volatile carbonyls, i.e., $Ni(CO)_4$ and $Fe(CO)_4$,

[2] Thermophoresis is the mechanism by which particles are transported in a fluid with a thermal gradient, i.e., from high temperature to low temperature. Therefore, particles are readily deposited on a cold surface—the TEM grid—when it is inserted in a hot gas containing the metal oxide particles.

[3] The dispersion of the Cu crystallites is defined as the ratio of surface Cu atoms to total Cu atoms.

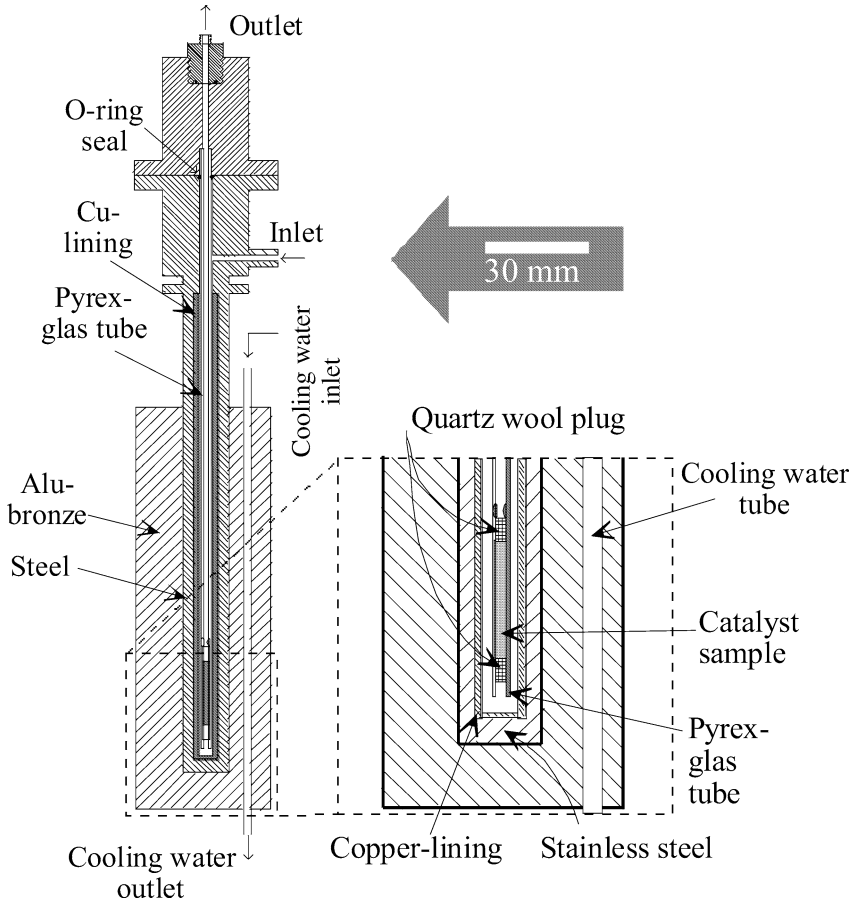

Fig. 5. Catalytic microreactor for testing of catalyst powder. All external units including pressure and flow controllers, active carbon trap, gas sampling valve, and the gas chromatograph are omitted from the drawing.

from CO in the feed gas, which pollute the catalyst with Ni and Fe.

The feed gas is drawn from a cylinder with a synthesis gas of fixed composition: 10% CO, 10% CO_2, and 80% H_2 with an impurity level less than 0.002%. The pressure of the reactor is controlled by a two-stage reduction valve at the feed cylinder. The flow of gas through the reactor is controlled by a flow controller for constant downstream pressure (Brooks 8842 with needle no. 1) positioned downstream from the reactor. The reactor pressure is monitored by manometers after the reduction valve and before the flow controller, respectively.

The product gas stream leaving the reactor is heated to 110 °C to avoid condensation of products. Downstream from the flow controller, at ambient pressure, the flow rate is measured by an optical/digital bubble flow meter.

The composition of the effluent gas is analysed by a Shimadzu GC-17A gas chromatograph. A 6-way gas sample valve with a 100-µl sample loop injects a gas sample into the carrier gas stream in which the organic compounds and the fixed gases are separated on two capillary columns and detected by a flame ionization detector and a thermal conductivity detector, respectively.

The GC is calibrated with gas standards of known composition.

Nickel carbonyl already forms at ambient temperature from the nickel in the stainless steel feed lines and the flow controllers. The feed gas must be purified in an active carbon filter to avoid a clearly discernible, gradual decline of the selectivity due to nickel poisoning of the catalyst (cf. Fig. 6).

The following standard test procedure is followed: The standard reaction conditions are 220 °C, 16 bar, and approximately 20 mg of catalyst loaded into the reactor. The feed flow rate is 25 $(N\,cm^3)$/min. Initially, the sample is reduced by increasing the temperature (20 °C/min) from room temperature to the reaction temperature while flushing the reactor with the feed gas (40 $(N\,cm^3)$/min).

The sample initially forms a packed bed within the glass capillary tube. Due to the small particle size, a pressure drop of several bars builds up to force the gas through the bed. The sample, however, shrinks on reduction by the reaction mixture during heating of the reactor, and the bed turns into a coherent, highly porous pellet with a narrow annular slit between the pellet and the glass wall for gas passage. The pressure drop subsequently becomes negligible and the reactor in fact is transformed into a single-pellet reactor with a

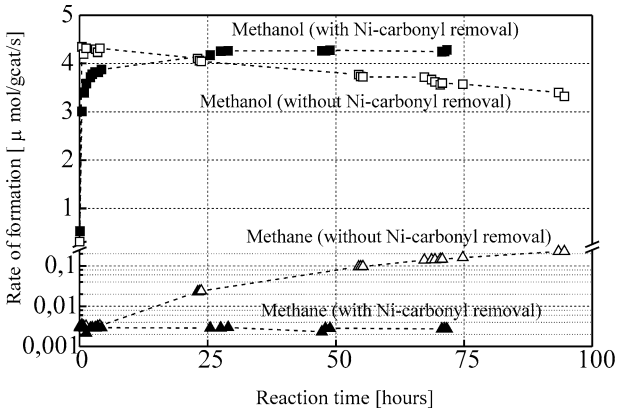

Fig. 6. Long-term test of catalyst activity and selectivity for catalyst "A" (cf. Table 2). The ordinate denotes the differential rates under the standard conditions: 220 °C, 16 bar, approximately 20 mg of catalyst and 10.0% CO, 10.0% CO_2, and 80% H_2. The figure also illustrates the influence of nickel poisoning of the catalyst before the nickel carbonyl trap was installed.

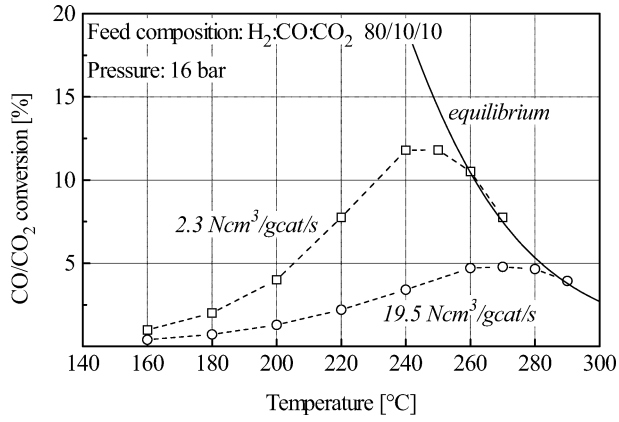

Fig. 7. X, T diagram for the methanol synthesis (cf. footnote 4).

cylindrical pellet with a diameter of 1.8 mm and a length of 20–30 mm.

The reactor is then kept at the standard conditions for 24 h and it is ascertained that the effluent gas composition has stabilized before the run is disrupted.

After the activity test, the copper dispersion is measured by N_2O titration, which is initiated by flushing the reactor with pure hydrogen for 1 h at 220 °C and 1 atm. The reactor is then cooled to 90 °C, at which temperature the N_2O titration is made as described in [7].

Fig. 7 shows the conversion X[4] for the carbon oxides as a function of temperature and space velocity for sample A of Table 2, which is the most active of the catalysts tested. The following two reactions describe the chemical changes in the gas:

$$CO_2 + 3H_2 \leftrightarrows 3CH_3OH + H_2O,$$

$$CO + H_2O \leftrightarrows 3CO_2 + H_2.$$

Both are exothermic, reversible reactions. In the X, T diagram of Fig. 7, both reactions are at equilibrium on the equilibrium curve, which for control of the chemical analysis is seen to be nicely approached by the measurements at high temperature. The activity measurements for the catalyst samples are all made at 220 °C and a space velocity of approximately 20 $(N\,cm^3)/(g_{cat}\,s)$. At these conditions, X is less than 2.5% and far below the equilibrium curve for all samples tested. The observed rate is hence the differential (or initial) rate measured at 16 bar and a composition approximately equal to the feed gas composition. The measured activity in Table 2 is shown as the molar rate of methanol production per gram of unreduced sample, or as the turnover frequency (TOF) defined as the molar rate of methanol production per mole of surface Cu.

We assessed the effect of pore diffusion on the measured activity by estimating values of the effective diffusivities and

[4] The degree of conversion is defined as $X = F_{Mf}/F_{CO}$ where F_{Mf} is the effluent methanol molar flow rate and F_{CO} total molar flow rates of $CO + CO_2$ in the reactor feed.

Table 2
Correlations between flame conditions, chemical composition, specific surface area, Cu dispersion, and catalytic properties

	Catalyst				
	A[a]	B[a]	C[a]	D[a]	E
Flame	H_2, quench	H_2, quench	H_2, quench	CH_4, quench	CH_4
Atomic ratio Cu:Zn:Al	45:45:10	50:50:0	50:0:50	45:45:10	50:50:0
BET surface area (m^2/g)	123	113	195	93	66
BET equiv. particle size (nm)	8.2	8.8	5.9	11.2	15.1
ZnO crystallite dimensions (nm)[b]	3.4	4.4	–	4.3	15.9
Copper dispersion (%)	8.9 (14.1)[c]	3.8	1.8	9.7	3.4
Cu surface area (m^2/g)	21.4	9.7	5.6	23.3	8.7
Estimated Cu particle size[d] (nm)	11.6	27	59	10.6	31
Activity ($\mu mol/(g_{cat}\,s)$)	3.66	1.61	0.27	1.99	1.07
TOF ($10^{-3}\,s^{-1}$)	7.1	6.8	2	3.5	5.1
SV ($cm^3/(g_{cat}\,s)$) (st. T, P)	19.2	19.2	20.7	19	16.5

[a] In the quenched flames, the quenched-air flow is 6.8 dm^3/min (25 °C, 1 atm).
[b] Dimension of the ZnO crystallites estimated using the Scherrer equation.
[c] Catalyst A has the Cu dispersion 14.1 when it is not exposed to synthesis gas prior to the N_2O titration.
[d] Based on overall copper content, Cu surface area and a density of solid copper of 8920 kg/m^3.

calculating the effectiveness factor for the actual reaction conditions, treating the catalyst bed as a cylindrical catalyst particle with a diameter of 2 mm [7]. The calculated effectiveness factor is between 0.9 and unity for all tests, which proves that the activity measurements are made under conditions of insignificant influence of pore diffusion. The effect of external diffusion resistance can also be neglected due to the narrow space available for gas flow in the cylindrical annulus surrounding the particle.

3. Results and discussion

Preliminary tests of the flame-generated ternary $Cu/ZnO/Al_2O_3$ catalyst prove that they are active and selective for methanol synthesis. The atomic ratio of Cu:Zn:Al = 45:45:10 represents a flat optimal activity for the flame-generated catalysts. The flame conditions, however, affect the observed activity significantly.

To clarify the role of each of the three constituent elements, we shall compare the ternary catalyst with the pure oxides and the three binary systems with respect to structure and catalytic properties for different flame conditions. Table 2 shows the samples which were prepared and tested with Cu as one of the components. Only those samples have potential for use as methanol catalysts. The activity per unit surface area is very low for both pure copper and pure ZnO, but in combination with a number of specific oxides and in particular ZnO, copper exhibits a strongly enhanced activity due to the so-called synergic promotion [13]. Table 2 includes the standard ternary catalyst and the Cu/ZnO binary catalyst, both for two different flame conditions and a single sample of the Cu/Al_2O_3 binary catalyst. Studies of flame-generated ZnO/Al_2O_3 particles are made by Jensen et al. [5] and particle properties for the pure oxides are studied by Jensen [7] and Jensen et al. [5].

3.1. Calculation of chemical and phase equilibrium

As an a priori assessment of the volatility and phase composition of the particles in the flame, we have calculated the simultaneous chemical and phase equilibria for the given overall flue gas composition.

The calculations are made by the method of Michelsen [14], which minimizes the total Gibbs free energy of a multicomponent, multiphase system at constant pressure and temperature subject to the conditions of a given content of elements. The gas is assumed ideal. All condensed phases are assumed immiscible so that each condensed component forms a separate pure solid or liquid phase. In the calculations we have attempted to include an exhaustive list of all possible vapour phase and condensed components which can be formed by the given elements in the flame. The thermochemical properties needed for the calculations are taken from published data sources [7]. Examples of equilibrium calculations are shown in Fig. 8 for the synthesis conditions of the ternary sample.

The calculations ignore both surface energy effects, which are potentially important for the stability of nanoparticles, and kinetic and diffusional effects, which may delay the actual attainment of equilibrium. However, in spite of these shortcomings, equilibrium calculations may still point to the likely identity of crystalline phases and volatile species formed at different temperatures and at least approximately identify the temperature ranges for the phase transformations. The limitations of the equilibrium approach is illustrated, though, by the fact that we have never identified the stable form of alumina, α-alumina, in the flame-generated nanoparticles. Evidently, the nucleation or stability of this alumina form is hindered in the small particles. α-Alumina is therefore not included in the calculations.

At the particle formation temperatures from 600 to 1500 °C, water has no influence on the thermodynamic sta-

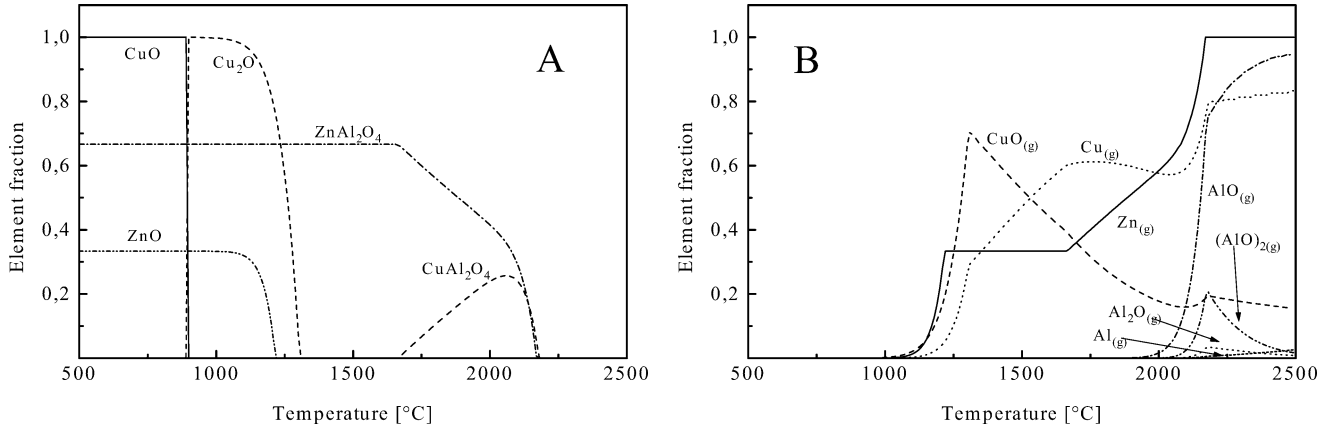

Fig. 8. Equilibrium distribution of elements in the $CuO/ZnO/Al_2O_3$ system between solids and an ideal gas phase as a function of temperature. The solid phases are shown in part A whereas the gas phase species are shown in part B. In this calculation α-Al_2O_3 is excluded from the possible phases. The moles of copper in the phases containing copper are normalized by the total moles of copper. The copper-containing phases therefore add up to 1. The zinc-containing species are normalized the same way. Phases containing aluminum only add up to unity at temperatures where none of the aluminum is bound in Cu- and Zn-containing species.

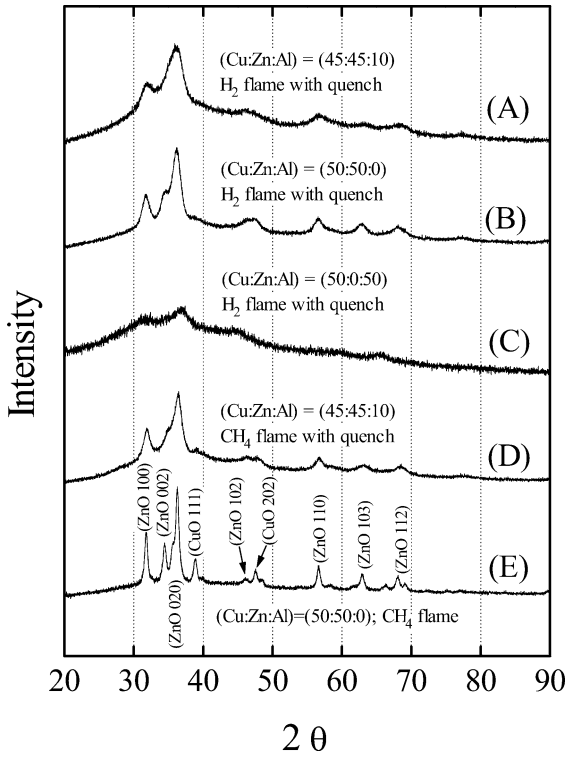

Fig. 9. X-ray powder diffractograms for the five samples of Table 2.

bility of the particles, and it is neglected in the equilibrium calculations.

3.2. Identification of phases

Fig. 9 shows the powder diffractograms for samples A–E of Table 2. The ZnO phase gives the strongest diffraction signal. In fact, almost all the identifiable peaks can be referred to ZnO. The same difference in signal intensity is seen for the binary samples. Only for sample E, separate CuO peaks are detectable in the diffractogram. The dispersion of the different phases increases when the flame temperature is decreased and when alumina is added to the sample.

3.3. ZnO/Al_2O_3 system

We have investigated the premixed-flame synthesis of particles of this binary composition quite thoroughly [5,7]. For the pure oxides ZnO and Al_2O_3 the specific surface area of the generated particles can be maximized by decreasing the flame temperature or decreasing the precursor vapour pressure. For Al_2O_3, surface areas in excess of 400 m^2/g can readily be obtained. The crystal structure is γ-alumina or X-ray amorphous depending upon the primary particle size. Particles synthesized in flames are usually crystallized in metastable phases such as γ- and δ-aluminas [1]. The structures of δ- and γ-alumina are related in that the long-range order has increased in δ-alumina. Further heat treatment of the δ alumina leads to formation of the stable α-phase. However, only the γ-phase was detected with certainty in this work. For ZnO the attainable surface areas are much smaller, i.e., in the range of 30–50 m^2/g. In XRD ZnO is wurtzite.

Particles of the binary ZnO/Al_2O_3 composition are characterized by the formation of the spinel phase of zinc aluminate $ZnAl_2O_4$, which for any overall composition appears to be formed to the full extent possible. The specific surface area increases considerably compared to that of pure ZnO when the overall composition contains even small amounts of Al_2O_3 and quite high and thermally stable $ZnAl_2O_4$ surfaces can be made in the premixed flame. Equilibrium calculations [7] substantiate that the $ZnAl_2O_4$ spinel is the most stable phase below approximately 2000 °C (provided α-Al_2O_3 is excluded from the calculation). The readiness and high yield with which $ZnAl_2O_4$ is formed in a single step from a homogeneous gas mixture proves the potentiality of the premixed flame for the synthesis of composite materials with high surface areas. The contribution of $ZnAl_2O_4$ to an increased surface area and thermal stability is a likely explanation of the beneficial role of alumina in the methanol synthesis catalyst.

3.4. CuO/Al_2O_3 system (sample C of Table 2)

The phase stability of this system resembles that of the ZnO/Al_2O_3 system. Equilibrium calculations show that either copper(II) aluminate ($CuAl_2O_4$) or copper(I) aluminate ($Cu_2Al_2O_4$) form stable solid phases for temperatures below 2200 °C [7]. The formation of $CuAl_2O_4$ is confirmed by XRD and seems to take place to the full extent possible for the given precursor composition [7]. Due to the low vapour pressures of the aluminates, the flame-synthesized particles consistently have high specific surface areas, which is the case indeed for the sample C subjected to catalytic test in Table 2. Evidently copper aluminate is an advantageous precursor for highly dispersed Cu because dispersions in the order of 25% was measured on samples of the CuO/Al_2O_3 particles after being cautiously reduced by He-diluted H_2 [7]. Therefore, the CuO/Al_2O_3 sample at first sight appears highly promising for Cu-catalyzed reactions and was indeed proven very active for the dehydrogenation of ethanol to acetaldehyde and ethyl acetate [7]. Unfortunately, the high Cu surface area rapidly deteriorates when exposed to elevated hydrogen partial pressures and in particular to the methanol reactant mixture [7]. In Table 2, sample C, in spite of a high BET surface area, has the lowest Cu dispersion. Although Cu/Al_2O_3 shows methanol synthesis activity, the Cu-based turnover frequency is clearly inferior to that of the ZnO-containing catalysts. The overall catalytic activity of sample C is therefore poor and the CuO/Al_2O_3 sample is of little interest for methanol synthesis.

3.5. CuO/ZnO system (samples B and E of Table 2)

Equilibrium calculations for this binary system [7] indicate that the solid phases are formed almost simultaneously

from the gas species Zn(g) and CuO(g) when the flame temperature is cooled below approximately 1000 °C. The stable solids are ZnO, CuO ($T < 600$ °C) and Cu_2O ($T > 600$ °C), of which ZnO is identified in the particles by XRD (Fig. 9)—CuO in sample E and vestigially in sample B.

There are no stable mixed oxide phases, but there seems to be a certain, although limited, solubility of CuO in ZnO [13], but basically the oxide phases of the two metals remain segregated either in separate particles or in composite particles with possibly only two different crystallites grown together.

For pure CuO the specific surface area is only moderately high and comparable to that of pure ZnO [7]. However, the binary particles tend to have surfaces larger than those of the pure oxides, probably because the immiscibility of the two oxide phases blocks for sintering at the contact points between unlike particles [7].

Two binary samples were included in the tests shown in Table 2. Both samples have a composition of CuO:ZnO = 1:1 but were synthesized at different temperatures and therefore subjected to different degrees of sintering. Sample E was synthesized in a high-temperature flame and has a lower BET surface area (66 m^2/g) than sample B (113 m^2/g), synthesized in a low-temperature flame.

Evidently, the higher temperature principally affects the ZnO phase of sample E because the ZnO crystallite size increases disproportionately more than the BET surface area decreases (Table 2). The CuO phase is probably less affected by sintering as evidenced by the comparable Cu dispersion (after reduction) for samples B and E. The growth of ZnO crystallites in the high-temperature flame possibly occurs subsequent to the initial particle formation as a secondary transport of vapours from small to large particles (Ostwald ripening). This was observed for the ZnO/Al_2O_3 system under similar conditions with ZnO in excess of that needed for the formation of aluminate [5]. In the low-temperature flame the secondary growth of ZnO crystallites is suppressed, not due to the lower peak temperature but rather to the faster cooling rate of the quenched hydrogen flame.

The high dispersion of the phases and the high specific surface area for sample B emphasize the importance of controlling the peak temperature of the flame to the lowest adequate level to avoid unnecessary sintering. The Scherrer crystallite size for ZnO is less than the equivalent particle size based on the BET area, which indicates that each particle consists of several crystallites grown together. For sample E there are identifiable XRD peaks for CuO (cf. Fig. 9). Their Scherrer crystallite size is 18.9 nm [7]. Thus, for sample E, generated at a high temperature, the crystallite sizes of ZnO and CuO and the BET-equivalent size are all three in the range of 15.1–18.9 nm, which seems to further illustrate the effects of excessive sintering in the high-temperature flame. This is also seen in Fig. 10 (right) where large, faceted crystals of ZnO appear on the TEM image. After reduction of sample E, the equivalent copper diameter is increased to 31 nm, so reduction of CuO to Cu for this catalyst is accompanied by an increase in size, probably by the coalescence of adjacent particles.

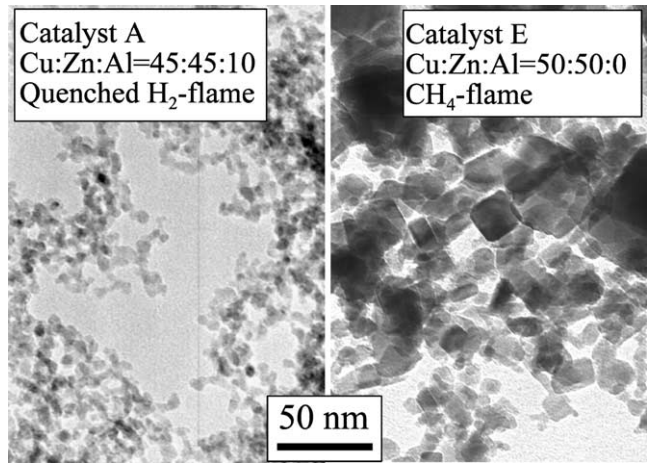

Fig. 10. Transmission electron micrographs of particles of samples A and E from Table 2, which shows the influence of aluminum and flame temperature on the phase dispersion. Sample A is generated at a low flame temperature with quenching and 10% aluminum and sample E at high flame temperature without quenching and no aluminum. In sample A the particles form dendritic clusters of coagulated very small primary particles. Sample E consists of separated individual crystals of ZnO (faceted, regular) and CuO (irregular). The chemical composition of the individual particles in sample A cannot be resolved due to limitations in resolution of the instrument.

The reduction of the CuO/ZnO samples (samples B and E) yields Cu dispersions considerably higher than that of the CuO/Al_2O_3 sample (sample C) in spite of the fact that the BET surface area of the latter sample is much larger. Together with the higher turnover frequency of catalysts B and E compared to catalyst C, this allows us to conclude that ZnO stabilizes the Cu crystallites formed by reduction and simultaneously modifies them chemically to be more catalytically active. The latter observation confirms a significant synergic promotion of ZnO in the flame-synthesized catalyst. The cause of the intensely investigated synergy between Cu and ZnO in the low-pressure methanol catalysts is as yet unsolved and is still open to the widely different interpretations (cf., e.g., [6,13,15]). These can be grouped into two classes: one in which the activity is related to the exposed surface area of the Cu crystallites, although the copper surface is modified by the presence of ZnO, and the other in which the active sites are Cu^+ cations dissolved in the ZnO crystals and the activity therefore is not related directly to the Cu surface area as determined by the N_2O method, but rather to the surface of ZnO. Catalysts B and E have very similar copper dispersions while the ZnO crystallite size is much larger for catalyst E. Since the copper-based turnover frequency is only slightly smaller for catalyst E than for catalyst B, the activity obviously does not depend on the ZnO surface, which is vastly different for the two catalyst samples.

3.6. $CuO/ZnO/Al_2O_3$ system (samples A and D of Table 2)

The ternary samples were synthesized in a high-temperature flame (D) and a low-temperature flame (A) with an overall composition of Cu:Zn:Al = 45:45:10. These two catalysts have the highest activity of all. The copper dispersion is approximately 10% for both reduced samples but the turnover frequency is higher for the catalyst synthesized at the low temperature, which thus yields the highest activity of the five catalyst samples.

Fig. 8 shows the calculated phase distribution at equilibrium for the overall composition of the ternary sample under the conditions in the flames, again with α-alumina excluded from the calculations. At temperatures above 1300 °C the aluminates $ZnAl_2O_4$ or $ZnAl_2O_4 + CuAl_2O_4$ are the only stable solid phases (Fig. 8A). Between 1300 and 1700 °C $ZnAl_2O_4$ is the most stable solid phase. Due to the molar ratio of zinc, copper, and aluminum (Zn:Cu:Al = 3:3:4) in the equilibrium calculation, $CuAl_2O_4$ is not present at equilibrium since all aluminum is bound as $ZnAl_2O_4$. Above 1700 °C $CuAl_2O_4$ appears in the equilibrium distribution in that Zn is vaporized. Below 1200 °C the volatility becomes negligible (Fig. 8B), and the oxides of Zn, Cu(II), and Cu(I) appear as additional, segregated solid phases (Fig. 8A). This provides the following likely mechanism for the gas-to-solid transformation in the flame: Immediately upon combustion solid $ZnAl_2O_4$ starts to form from the highly supersaturated Al species in the gas. This leads to dendritic aggregates of small coagulated primary aluminate particles (cf. Fig. 10, left). As the flue gas cools, the saturation points for the pure oxides of Zn and Cu are reached and the oxides start to condense, however in a more gradual way, controlled by the cooling rate. The oxides presumably nucleate and grow at the large surface of the initially formed aggregates of $ZnAl_2O_4$. The final pelletized sample thus attains a structure with a $ZnAl_2O_4$ skeleton with alternating crystallites of CuO and ZnO intimately mixed along its surface.

This structure combines the beneficial features discussed above for the CuO/ZnO and CuO/Al_2O_3 samples and the ZnO/Al_2O_3 system. It ensures an intimate contact between Cu and ZnO and a large and stable surface area of $ZnAl_2O_4$, which binds Al, so that the formation of copper aluminate with its poor catalytic properties is prevented. The copper particle size after reduction is close to the BET-equivalent diameter for samples A and D. Evidently, the ternary catalyst, to a higher degree than the other catalysts, protects the copper particles from growing during reduction from CuO to Cu.

The theory, that Cu_xO nucleates independently of the other species at temperatures well below the peak temperatures of the flame, is corroborated by the fact that the copper dispersion is almost independent of the flame conditions for both the CuO/ZnO (samples B and E of Table 2) and the $CuO/ZnO/Al_2O_3$ catalyst sample (samples A and D). In both the binary and the ternary sample, however, the ZnO crystallite size is larger in the methane flame than in the hydrogen flame. This can be explained by a secondary growth of the ZnO crystals in the ternary system equivalent to that of the binary case as discussed above. The turnover frequency is moderately lower for the catalyst from the methane flame for both the binary and the ternary catalyst, which may be caused by the larger ZnO crystallite size. It explains why catalyst D has the poorer activity of the two ternary catalysts, in spite of the fact that they have approximately the same copper dispersion.

The contribution of aluminum and a low flame temperature in the creation of a high dispersion of the phases is evident from Fig. 10, which compares the TEM images of samples A and E.

3.7. Catalyst stability

Catalyst A of Table 2 in addition to the standard activity test has been subjected to further tests as shown in Figs. 6 and 7. The stability of the catalyst was measured over a 4-day period, during which the reactor was operated continuously at the standard test conditions. The differential rate of reaction as a function of time is shown in Fig. 6. The figure also shows the effect of Ni-carbonyl poisoning of the catalyst which gave rise to installment of the active carbon trap. Without the trap installed, the activity slowly decreases and the undesired methane production increases. With the trap installed, the activity after an initial increase over 24 h remains constant for the whole test period. The test was concluded by a 4-h rise of the temperature to 290 °C, which has no effect on the activity measured subsequently at the standard temperature. Fig. 6 also demonstrates the excellent selectivity of the catalyst. Methane, which is the only detectable by-product of the reaction, is produced in minute amounts unless the catalyst is contaminated by Ni.

3.8. Future work

Future work on this catalyst may include an attempt to optimize the catalytic properties of the prepared samples by adjustment of the flame synthesis conditions. This study would also require a more careful control of the reduction process in that the activity of the final catalyst presumably is very sensitive to the reduction conditions.

4. Conclusion

Flame combustion synthesis has been proven to be a versatile method for producing metal-oxide catalysts with large specific surface areas.

The specific surface area, structure, and phase composition of the product materials are significantly affected by the flame conditions and the burner design. Thus, immediate alterations in the properties of the effluent particles can be effected by simple adjustments of the operating conditions. There are many possibilities for optimizing product

properties and developing materials, tailormade for specific purposes.

The premixed flame, in which fuel, air, and several different volatile precursor species are all mixed together prior to combustion, provides a homogeneous temperature environment for the particle synthesis since all precursor species traverse the high-temperature zone. The premixed flame is shown to be ideally suited for the synthesis of nanostructured mixed oxide phases like, e.g., spinels, which are produced in a single step, which means that no further, surface reducing thermal treatment is necessary. The material properties obtainable by combustion synthesis are particularly attractive for catalytic materials.

It is shown in this study that flame combustion synthesis can generate a $Cu/ZnO/Al_2O_3$ catalyst for methanol synthesis with very high activity, selectivity, and stability. The study also demonstrates how the versatility of the flame reactor can be used to affect fast, systematic changes in catalyst composition and structure, which is useful in the study of how the structure of a catalyst affects its catalytic behaviour.

Flame synthesis of catalysts may find a more widespread use in catalytic research due to the versatility of the method. It is, as yet, quite untested in large-scale catalyst manufacture. In the laboratory, the process presently appears rather expensive and has a rather low production rate. However, today some materials (TiO_2, carbon black, SiO_2) are already manufactured in large quantities by industrial flame synthesis. An optimized scale-up of the laboratory process possibly may lead to competitive manufacturing processes also for catalytic materials.

It is also possible that flame combustion may find a special application in the manufacture of, e.g., catalysed hardware, i.e., surfaces of process equipment with thin coatings of catalyst, or catalytic membranes. Both applications are presently under investigation in our laboratory.

Acknowledgment

This work was funded by the Danish National Research Councils.

References

[1] S.E. Pratsinis, Prog. Energy Combust. Sci. 24 (1998) 197.
[2] M.S. Wooldridge, Prog. Energy Combust. Sci. 24 (1) (1998) 63.
[3] W.J. Stark, K. Wegner, S.E. Pratsinis, A. Baiker, J. Catal. 197 (1) (2001) 182.
[4] T. Johannessen, S. Koutsopoulos, J. Catal. 205 (2002) 404.
[5] J.R. Jensen, T. Johannessen, S. Wedel, H. Livbjerg, J. Nanoparticle Res. 2 (4) (2000) 363.
[6] J.B. Hansen, in: G. Ertl, H. Knözinger, J. Weitkamp (Eds.), Handbook of Heterogeneous Catalysis, Vol. 4, Wiley–VCH, Weinheim, Germany, 1997, p. 1856, Chapt. 3.5.
[7] J.R. Jensen, Flame synthesis of composite oxides for catalytics applications, PhD thesis, Department of Chemical Engineering, Technical University of Denmark, 2001.
[8] J.P. Hansen, J.R. Jensen, H. Livbjerg, T. Johannessen, AIChE J. 47 (2001) 2413.
[9] H.P. Klug, L.E. Alexander, X-Ray Diffraction Procedures—For Polycrystalline and Amorphous Materials, Wiley, New York, 1974.
[10] G.C. Chinchen, C.M. Hay, H.D. Vandervell, K.C. Waugh, J. Catal. 103 (1987) 79.
[11] J.W. Evans, M.S. Wainwright, A.J. Bridgewater, D.J. Young, Appl. Catal. 7 (1983) 75.
[12] S. Sato, R. Takahashi, T. Sodesawa, K. Yuma, Y. Obata, J. Catal. 196 (2000) 195.
[13] K. Klier, Adv. Catal. 31 (1982) 243.
[14] M.L. Michelsen, Fluid Phase Equilib. 53 (1989) 73.
[15] A.Y. Rozovskii, G.I. Lin, Kinet. Catal. 40 (6) (1999) 773.